Effects of a grain boundary on the photoluminescence spectrum of silicon: expansion of electron-hole droplet cloud

1995 J. Phys.: Condens. Matter 7 6161

(http://iopscience.iop.org/0953-8984/7/30/018)

J. Phys.: Condens. Matter 7 (1995) 6161–6177. Printed in the UK

Effects of a grain boundary on the photoluminesence spectrum of silicon: expansion of electron–hole droplet cloud

Richard Rizk, Roger Madelon and Francis Cruège

Laboratoire d'Etudes et de Recherches sur les Matériaux (LERMAT), CNRS URA 1317, Institut des Sciences de la Matière et du Rayonnement (ISMRA), Campus Universitaire II, 6 Boulevard du Maréchal Juin, F-14050 Caen Cédex, France

Received 18 January 1995

Abstract. Spatially resolved photoluminescence (PL) experiments on $\Sigma = 25$ silicon bicrystals have been performed at very low temperatures (~ 4.2 K) for the first time. Owing to the focusing mechanism required for high spatial resolution, the concomitant increase of the pumping power, P, has led to the emergence of an electron–hole droplet (EHD) PL band besides the usual free-exciton (FE) line. The effects of the grain boundary (GB) of both as-delivered and heat-treated specimens were investigated by additional scanning of the bicrystal by the exciting laser beam across the interface. For the annealed as-received or deliberately contaminated samples (with Cu), the scan profiles of the maximum intensities emitted by the EHDs and FEs were symmetrical with respect to the GB and have revealed a smooth increase followed by an abrupt drop upon approaching the interface. While the PL enhancement is interpreted in terms of the existence of a denuded zone, exempt from non-radiative channels, on either side of the boundary, the built-in electric field due to GB precipitates is thought to dissociate the condensed and free excitons leading to the above-mentioned steep decrease around the boundary. A complete modelling of these effects has been carried out for the case of EHD and the reproduction of the related scan profiles has allowed the determination of the effective lateral expansion, L_{eff}, of the EHD cloud, as well as a rough estimate of the average drift velocity, v_d, of the droplets. The reported variation of L_{eff} with P, exhibiting a fairly good $P^{1/3}$ dependence as established earlier by Bagaev and co-workers and explained in terms of a phonon wind mechanism, signifies a nearly linear expansion of the cloud volume with laser power and, therefore, an almost constant filling factor of the cloud by the generated droplets. Furthermore, the evolution of v_d from 1.4×10^4 to 3.5×10^4 cm s^{-1} when P varies from 7 to 500 mW provides further confirmation for the droplet transport being mainly due to the so-called phonon wind. Finally, the behaviour of EHD and FE scan profiles in the as-grown samples is interpreted in terms of stresses and strains developed by the lattice distortion in the close vicinity of the GB.

1. Introduction

Extensive studies have been devoted during the past decades to the investigation of electrical activities and structural configurations of grain boundaries (GBs) in semiconductors [1, 2]. In this connection, the particular interest attached to the role of boundaries as gettering centres for diffusing metallic contaminants in silicon is essentially due to the subsequent drastic changes in the electronic properties of the material. On the other hand, as far as we know, none of the optical spectroscopic techniques has been used to establish the effects of the GB on the photoluminescence (PL) spectral lines following the role played by other extended defects such as dislocations [3, 4]. For this purpose, we have undertaken a spatially resolved PL study by means of sample scan by the exciting laser beam. The focusing mechanism required for the spatial resolution investigation inevitably induced an

0953-8984/95/306161+17$19.50

increased power density which, in turn, obviously led to the emergence of the characteristic electron–hole droplet (EHD) band on the low-energy side of the usual free-exciton (FE) line [5].

Considerable effort has been supplied in the 1970s [5] and the early 1980s [6–8] to the investigation of the condensed EHD phase in crystalline Si and Ge. Apart from a reasonable understanding of the structure of EHDs in these materials, little is known about their motion and spatial distribution. In Ge, the droplets, each between 2 μm [9] and 10 μm [10] in size, were found to be spatially distributed, following a certain gradient density [11], in a cloud of macroscopic size (a few millimetres) [9]. However, besides the unique estimate of the droplet size (~ 0.75 μm) in Si [12], only one experiment, using the slit scan technique, was performed with the aim of determining the spatial extent of the EHD in this material [13]. The difficulty in such measurements for the case of Si seems to lie mainly in the relatively short lifetime (140 ns) of its droplet [14] compared to that (40 μs) in Ge [15], which results in some shortening in the propagation of these droplets in Si. According to an early suggestion by Keldysh [16], which was subsequently supported by the experiment of Bagaev *et al* [17], the EHDs are dragged by a 'phonon wind' (short acoustic waves) arising from carrier thermalization in the excitation point (T phonons) and from the non-radiative recombination of e–h pairs in each droplet (R phonons). While the T phonons tend to propel the droplets away from their point of generation, the R phonons, emitted from each droplet, can be absorbed and scattered by the surrounding droplets. Accordingly, the droplets are mutually repelled [7] in such a way that the R phonon transport effects might be opposed to those of T phonons in the cloud expansion. Some studies [18] have concluded that the relative amounts of T and R phonons have a clear influence on the size of the cloud.

In the present paper we report some striking effects of a $\Sigma = 25$ GB on the PL spectrum of silicon. We have basically made use of a well-defined model system offered by the twin boundary in a specially grown silicon bicrystal [19], which allowed the deduction of the lateral expansion of the EHD cloud size. This latter has been determined by the modelling of the EHD intensity scan profile across the $\Sigma = 25$ GB of the heat-treated silicon bicrystal whose electrical activity has been attributed predominantly to the metallic impurities precipitating at the boundary and which behave as a multicarrier amphoteric trap [20]. In recent papers [21,22], we reported on the evolution of the electrical activity, i.e. barrier height and interface state(s), of the same and identically heat-treated sample either with a gradual increase of the contaminant (Cu and/or Ni) or with the heat treatment temperature. Beside the absence of barrier effects in the as-grown sample, we have shown evidence of the rectifying behaviour of the 'buried' metallic precipitates, formed at the GB upon heat treatment, which reveal themselves in this work by the dissociation of the neighbouring exciton particles. Some preliminary results of the present study have been given recently [23], where they were particularly compared to electron-beam-induced current (EBIC) measurements.

2. Experimental details

The samples used in this study were cut from a $\Sigma = 25$ silicon bicrystal in the shape of a rectangular parallelepiped ($10 \times 6 \times 0.3$ mm^3) with the GB plane perpendicular to the longer dimension. The geometrical parameters of the twin consist of a {710} plane boundary, 16.26° tilt angle, and a common ⟨001⟩ tilt axis. The bulk material was Czochralski-grown (CZ) n-type (phosphorus doped at $N_d = 3.1 \times 10^{14}$ cm^{-3}) and was found to contain 5×10^{17} cm^{-3} and 0.75×10^{17} cm^{-3} of oxygen and carbon, respectively. The heat treatment of each of

the as-delivered and intentionally copper-contaminated samples was carried out in an open quartz tube furnace under a continuous flow of pure argon at 900 °C for 3 h. The samples were subsequently quenched by their rapid withdrawal to the cold end of the quartz tube. Both surfaces of the samples were then mechanically polished with a paste of small-sized diamond grains down to 3 μm size for the back side and to 0.25 μm size for the illuminated side. They were cleaned sequentially in trichloroethylene, acetone and methanol ultrasonic baths and then dried. In order to reduce further the surface recombination, a final chemical etching was performed in an acid solution of $HNO_3/CH_3CO_2H/HF$ (16/3/1) before being rinsed with methanol and dried.

The photoluminescence (PL) measurements were performed at low temperatures (near 4.2 K) with the sample mounted on an Air Products cryostat (Model LT 3-110). The scanning by the laser beam was accomplished by means of a motorized uniform translational displacement of the sample with a speed of 3 mm h^{-1}. The sample was excited with a finely focused laser ($\lambda = 0.660$ μm) spot approximately 5 μm in diameter on the mirror-like polished surface. At 0.660 μm the silicon absorption coefficient is about 2×10^5 cm^{-1} at low temperatures ($\sim$ 4.2 K) and the penetration depth is near 5 μm [24]. This ensures a somewhat 'volume' generation, expected to be slightly affected by any surface recombination. The spatial resolution, as defined by the spot radius at $1/e^2$ intensity point, was determined through deconvolution of the intensity distribution profile measured in the scanning over a well defined edge of the sample. Details concerning the experimental procedure and the determination of the spatial resolution are published elsewhere [25]. The luminescence emission was detected by a 77 K cooled Ge photodetector after dispersion by a 1 m grating monochromator. The spectrum characteristic of each sample was recorded during a PL scan from 0.775 to 1.170 eV.

3. Results

Figure 1 shows a typical TO–LO replica of PL spectra obtained at low temperatures for a laser power of 7 mW. Both EHD (at 1.080 eV) and FE (at 1.097 eV) lines can be observed at intermediate low temperatures whereas only one phase appears predominant at lower and higher temperatures, namely EHD at 4.2 K and FE at 13.5 K, for the incident power used. This behaviour confirms the interpretation of a first-order liquid–gas phase transition [26, 27]. The sample temperature was compared to that obtained from a fit of the FE luminescence band [6]. The FE temperature was found to exceed the measured temperature by $\leqslant$ 0.5 K. This temperature was checked at 4.2 K by fitting the EHD band after the approach of Hammond *et al* [28].

The spectra displayed in figure 1 are basically valid for all the samples used in this study, i.e. the as-grown (sample A) and heat-treated samples whether they are unintentionally contaminated (sample B) or deliberately contaminated with copper (sample C). As a fast diffuser in silicon, copper is thought to be an easy and almost 'unavoidable' contaminant [29, 30]. This explains why we investigated the influence of impurities precipitating at the boundary towards the PL spectrum on samples precontaminated with copper. In figure 2, we compare the PL spectra related to the aforementioned samples, as recorded at 4.2 K for a power of 40 mW. While the luminescence yield appears notably improved after heat treatment of the as-delivered sample (compare spectra (*a*) and (*b*)), the PL emission from sample C (spectrum (*c*)) is fourfold that of its uncontaminated counterpart (sample B, spectrum (*b*)). It is worth pointing out that this enhancement in the PL emission might originate mainly from an increase in EHD nucleation caused by copper point defects, and

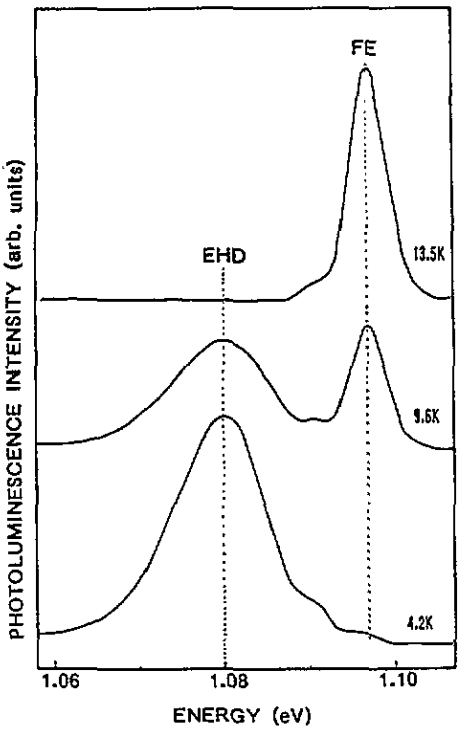

Figure 1. *Typical PL spectra of silicon for a highly* focused laser spot at 13.5 K, 9.6 K and 4.2 K. The excitation power was 7 mW. Peaks at 1.080 and 1.097 eV correspond to LO- and TO-phonon-assisted recombination of the condensate (EHD) and gaseous (FE) phase, respectively. For the sake of clarity, the spectra are shifted vertically.

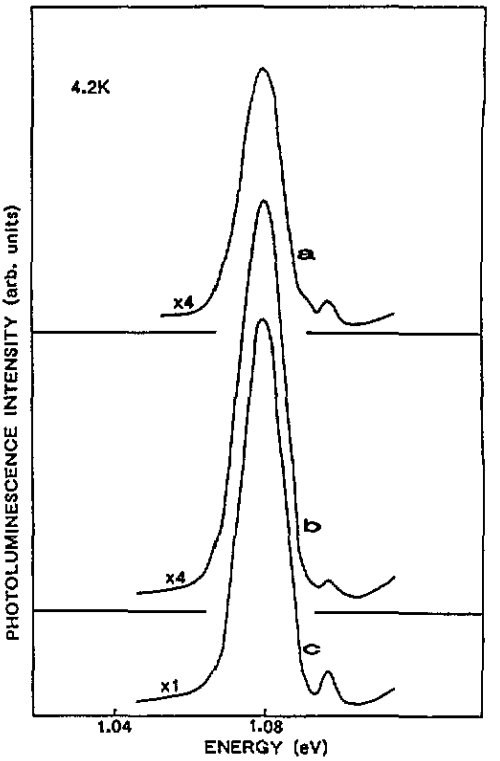

Figure 2. *PL spectra of the as-grown* (sample A, spectrum (*a*)) and heat-treated samples. The latter consist of unintentionally contaminated (sample B, spectrum (*b*)) and deliberately contaminated with copper (sample C, spectrum (*c*)). The measurements were performed at 4.2 K with a laser power of 40 mW.

to a lesser extent by the well-known internal gettering of impurities in our CZ-Si [31] that would reduce the non-radiative centres. A detailed investigation of these features however is beyond the scope of this work.

Figure 3 shows the variations at 12 K of the maximum intensities, I_M, of the FE (curve (*a*)) and EHD (curve (*b*)) emission, respectively, along a line scan from right to left across the GB of sample B, for an output power of 35 mW. No shift of the energy peak positions has been found all along the scan. Besides the remarkable symmetry of the scan profiles of I_M with respect to the GB plane, one can notice the drastic decrease on both sides of the GB that arises at different distances from the interface for EHD and FE. Another important feature concerns the monotonic increase preceding the mentioned abrupt decline, which starts in both cases at about the same distance ($\sim$ 150 μm) from the boundary. For the EHD line (curve (*b*)), this increase is combined with some reproducible smooth modulation. The EHD and FE scan profiles recorded on sample C (contaminated with Cu) exhibited the same overall shape as the corresponding ones (curves (*a*) and (*b*)) obtained on sample B. The only difference that one may distinguish in the profiles of the two types of specimens B and C concerns a more marked raising of the luminescence

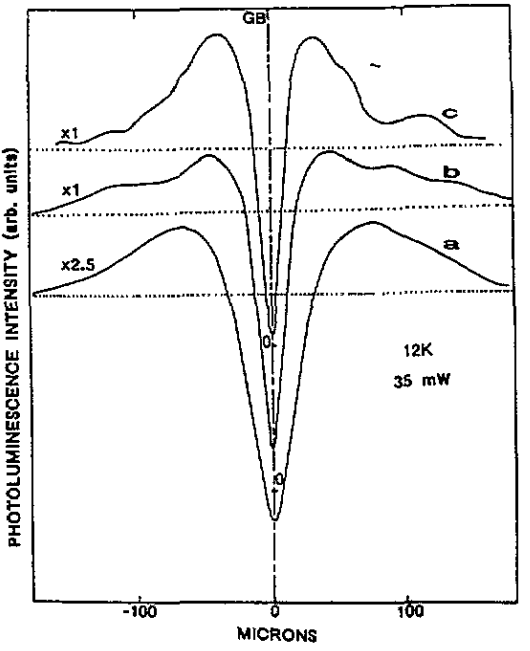

Figure 3. Line scans across the GB plane of the as-received and heat-treated specimen (sample B), relative to the PL intensities at 12 K with the selected energies 1.097 eV (FE: curve (*a*)) and 1.080 eV (EHD: curve (*b*)). The EHD line scan for the Cu-contaminated specimen (sample C) is also reported (curve (*c*)) for comparison. The excitation output power was 35 mW. The curves are shifted vertically.

efficiency preceding the tremendous collapse, as illustrated by the comparison of curve (*b*) to its counterpart curve (*c*) (figure 3) that reproduces the EHD profile for sample C. The Cu-related spectral lines were detected only in sample C, i.e. that deliberately contaminated with Cu. Figure 4 shows the Cu_0^0, Cu_0^1, Cu_0^2 and Cu_0^3 lines at 1.0141, 1.0074, 0.9998 and 0.9926 eV, respectively, in nearly perfect agreement with the analogous ones previously reported by Weber *et al* [32]. The structure of the high-energy edge of the Cu_0^0 band is recognized as the two-phonon EHD replica [33]. The scan profile of the 1.0141 eV peak across the GB plane (not shown) has been recorded at 15.8 K, a temperature that tends to remove the EHD phase whose presence hides the actual line scan of the Cu-related band through the adjoining phonon replica. It shows a fairly regular height of the 1.0141 eV peak all along the line scan. Within the limits of our spatial resolution, this is indicative of a somewhat uniform distribution of the *radiative* Cu-based centres around the GB.

Figure 5 shows the analogous measurements performed on sample A (as-grown) as recorded at a temperature corresponding to either the coexistence of both EHD and FE phases, for instance 12 K (figure 5(*a*)), or to the prominence of one of them such as 4.2 K for EHD and 15.7 K for FE (figure 5(*b*)). Besides the symmetry of the scan profiles towards the GB plane in the former case (figure 5(*a*)), reminiscent of that noticed for the similar line scans on the heat-treated samples (figure 3), one can emphasize the striking complementary changes between both EHD and FE emissions. By contrast to their counterparts shown for annealed samples (figure 3), these changes occur in much closer vicinity of the GB and show an EHD or FE intensity at the GB level, almost equivalent to that in the bulk. The full width at half-maximum or minimum (FWHM) of the central part of I_M variations is

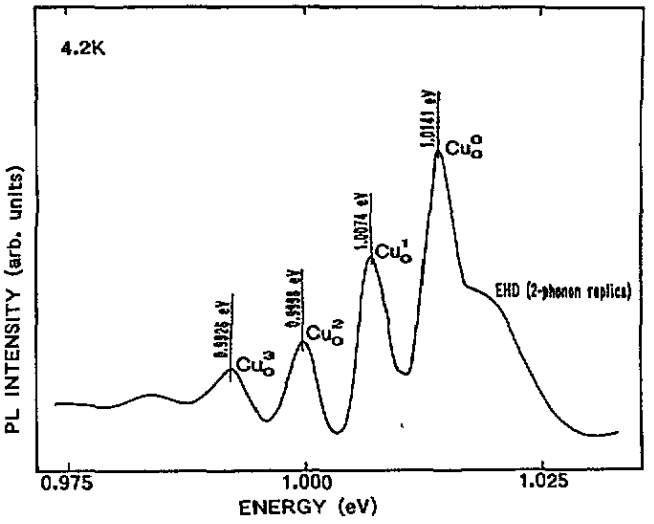

Figure 4. Characteristic PL spectral lines recorded at 4.2 K of Cu-related recombination centres in Cu-contaminated silicon. As labelled by Weber *et al* [32] Cu_0^0 is the no-phonon transition, while Cu_0^1, Cu_0^2 and Cu_0^3 are the lower-energy resonant-mode phonon replicas with an equal interval between them of 7.0 meV, the typical phonon energy. The high-energy sided shoulder of the Cu_0^0 line is the EHD replica involving a two-phonon combination as previously identified by Vouk and Lightowlers [33]. The spectral resolution was less than 0.5 meV.

of the order of a few micrometres and is then a clear indication of the spatial resolution of our experimental set-up. However, only small changes in EHD strength are revealed around the GB (figure 5(*b*)) at the temperature of 4.2 K where the gaseous phase is absent. The corresponding scan profile for FE, recorded at 15.7 K (figure 5(*b*)) where the liquid phase has vanished, is different and somewhat opposite to the FE profile recorded at 12 K. Although these features will be tentatively explained in section 5, these results seem to suggest that the behaviour of either EHD or FE emission in the vicinity of the GB of the as-grown sample is governed mainly by the simultaneous presence of the opposite excitonic phase.

4. Model

As mentioned before, the reproduction of the scan profiles has been efficiently achieved for the heat-treated samples. This enables us to deduce the EHD characteristics (cloud expansion, droplet velocity). Thus, in order to lay the basis of this quantitative study, it is useful to give first a qualitative explanation of the effects involved by the scan profiles of figure 3.

The numerous capacitance measurements reported previously by Broniatowski *et al* [20, 30, 34, 35] and recently by us [21, 22] on the same $\Sigma = 25$ and identically heat-treated sample provide definite evidence of the existence of a potential barrier at the GB, i.e. a built-in electric field, due to metallic precipitates at the GB plane, which behave as a metallic film between the two grains resulting in a configuration of Schottky diodes back to back [20–22]. Furthermore, we have found [21] that the electronic properties of B and C samples are characterized by a single or continuous distribution of interface trap

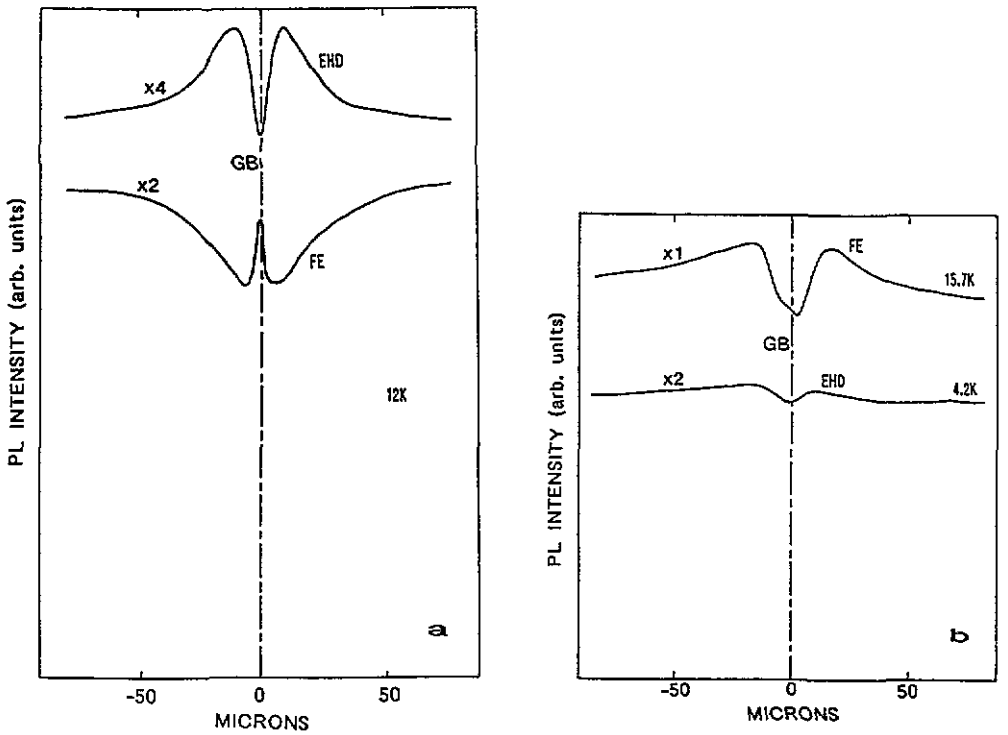

Figure 5. PL line scans across the GB plane of the as-grown specimen (sample A) at the selected energies 1.080 eV (EHD) and 1.097 eV (FE) for a laser power of 38 mW. In (*a*) both scans were performed at 12 K where the condensed and gaseous phases coexist. In (*b*), each scan is recorded at the temperature corresponding to the existence of one of the two phases: 4.2 K for EHD and 15.7 K for FE.

state(s) lying in the upper half of the band gap with an average density of states of a few 10^{11} cm^{-2}. On the other hand, the transmission electron microscopy (TEM) observations performed by these authors [20, 30, 35], as well as by us [21], have shown that these metallic precipitates are mainly copper silicides (Cu_3Si) originating from either unintentionally [30] or voluntarily incorporated copper [20, 21, 35, 36] and are disc-shaped particles gathered in circular colonies at the GB plane. At the same time, these TEM observations do not detect any precipitate or any defect in the region adjacent to the GB up to a distance of several tens of micrometres away from the interface [35]. The existence and extent of such a defect-free denuded zone (DZ) on both sides of the GB have been confirmed by our recent electron-beam-induced current (EBIC) measurements performed on the same sample [23]. Because of the limitation of our facilities, EBIC measurements at low temperatures were beyond reach, although the available deep-level transient spectroscopy (DLTS) technique has already allowed us to detect the interface deep states. The DZ was found to extend to a distance of ~ 150 μm [23] which matches well with that corresponding to the start of the PL increase (figure 3). Consequently, the gradual enhancement of the emission preceding the abrupt decrease can be ascribed to the reduction of the non-radiatively recombining centres due usually to existing impurities [37]. This is supported by the consistency between the smooth increase of the luminescence efficiency upon approaching the interface (full lines of figure 6), and the expected gradual improvement in the GB gettering efficiency. As for the

absence of alteration in the distribution of radiative Cu centres by the GB, it might be due to the saturation of the boundary by the impurity precipitates since these Cu-related lines are detected in samples oversaturated by copper [32].

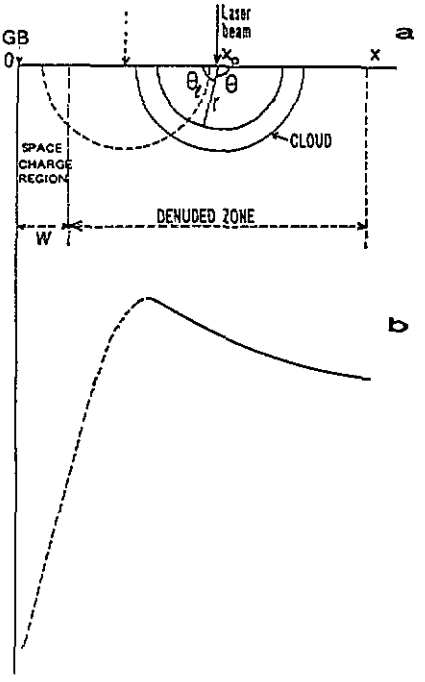

Figure 6. (*a*) Schematic representation of the cloud displacement accompanying the scanning of the grain boundary (GB) from right to left. The full line corresponds to a cloud located entirely outside the space charge region (SCR), whereas the dashed line represents the case where there is an overlap between the cloud and the SCR. w is the one-side width of the depleted zone, r and θ are the radial and angular coordinates of a droplet, respectively; x_0 is the laser beam position. (*b*) Schematic representation of the corresponding variation of the maximum intensity of the EHD profile in the denuded zone (full line) and when the EHD cloud reaches and enters the SCR region (dashed line).

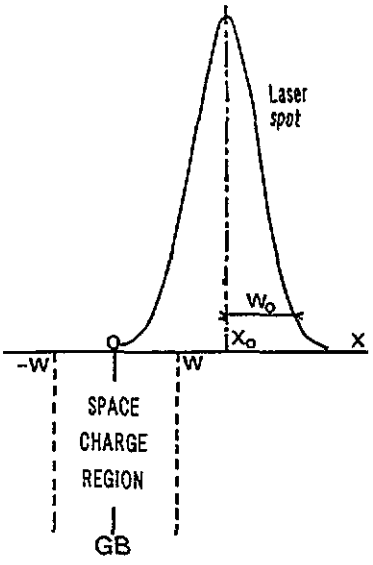

Figure 7. Illustrative sketch of the overlap case between the spot extent and the space charge region extending to w over each side of the grain boundary (GB); w_0 is the half-width of the spot at $1/e^2$ of the maximum.

However, the above-mentioned improvement in the PL yield ceases to prevail as soon as the edge of the excitonic cloud enters the space charge region (SCR) (dashed lines in figure 6(*a*)) developed by the 'buried' Schottky diode constituted by the precipitates at the boundary [20–22]. The condensed and free excitons are then dissociated by the SCR electric field [12, 38] and the resulting free carriers would subsequently be either trapped or non-radiatively annihilated by the precipitate, leading to the pronounced decrease in I_M down to a marked minimum at the boundary (dashed line of figure 6(*b*)). The fact that we are dealing with minima not equal to zero can be understood by considering that the extent of the laser spot used is larger than the depleted layer width. In the case of a spot entering the SCR, it appears obvious that the excitons created within the depleted zone are

instantaneously dissociated and then lost, whereas those generated outside the SCR continue to be detected.

We shall first examine the general case of carrier generation occurring entirely outside the SCR. This corresponds to the situation where the laser spot is beyond the band bending area, where it is helpful to start by determining the behaviour of the luminescence enhancement in the DZ which we associated above with the 'clearing' of that zone from non-radiative impurity centres. In this connection, since the solubility of the impurities is highly dependent on the temperature, it is clear that, upon cooling, these contaminants would be firmly ejected from the grains towards the nearest defects such as dislocations, cavities and GBs where the free energy is more important than in the bulk [39]. This energy excess is at the origin of the precipitation of diffusing impurities at the GBs that act as 'gettering' sites. In this way, the so-called DZ appears on either side of the GB, where the concentration of impurities or non-radiative centres is reduced by the gettering process, whereas this concentration increases with distance from the interface until it recovers its value in the bulk. The mechanism governing this behaviour may be described as follows:

In a one-dimensional and symmetrical system, with respect to an origin, $x = 0$, taken at the GB position, the net migration 'current' of impurities (of concentration n) flowing in the $x < 0$ direction may be written as:

$$\mathrm{d}J = -[(vn)_{x+\mathrm{d}x} - (vn)_x] \tag{1}$$

where v is the migration velocity.

During the cooling time interval δt, the amount of impurities crossing unit area is $\delta t\,\mathrm{d}J = \delta n\,\mathrm{d}x$. Assuming a constant migration velocity in all the denuded zone, equation (1) then implies that:

$$\frac{\delta n}{\delta t} = -v\frac{\mathrm{d}n}{\mathrm{d}x} \tag{2}$$

The right-hand side of equation (2) must be added to that due to diffusion:

$$\frac{\partial n}{\partial t} = D\frac{\mathrm{d}^2 n}{\mathrm{d}x^2} - v\frac{\mathrm{d}n}{\mathrm{d}x} \tag{3}$$

where D is the diffusion coefficient. At equilibrium where $\partial n/\partial t = 0$, the solution of the preceding equation indicates an exponential decrease such as $n \propto \exp(vx/D)$ upon approaching the GB.

Accordingly, the luminescence efficiency ε, whose evolution could be reasonably taken as the inverse of that of the impurity concentration in the denuded zone, may be assumed to vary following the relation:

$$\varepsilon(x) = \varepsilon_0 + \alpha \exp(-x/\sigma) \tag{4}$$

where ε_0 is the luminescence efficiency in the bulk (i.e. beyond the denuded zone), and α and σ are the characteristic parameters of the exponential variation of $\varepsilon(x)$. The PL intensity is then calculated according to the convolution integral:

$$I(x_0) = \int \varepsilon(x) n(r)\,\mathrm{d}^3 r \tag{5}$$

where $n(r)$ is the spherically symmetric distribution of the density of drops or excitons at a distance r from the isotropic centre of generation assumed to be at the sample surface

where the laser is focused, i.e. at $x = x_0$. The drops distribution has been derived by Bagaev *et al* [17] in terms of the phonon wind mechanism and is found to obey the relation:

$$n(r) = n_0 \exp(-r/L_{eff})^3 \tag{6}$$

where n_0 is the density at the excitation point and L_{eff} the effective spatial extent of the cloud. This latter depends on the phonon flux which in turn varies with the excitation power P. According to the same authors [17], $L_{eff} \propto P^{1/3}$ and the cloud volume is expected to expand linearly with the absorbed laser power.

With appropriate spherical coordinates around x_0, (figure 6(a)), equation (5) becomes:

$$I(x_0) = \pi \int_0^\infty n(r) E(r, x_0) r^2 \, dr \tag{7}$$

where

$$E(r, x_0) = \int_0^{\pi - \theta_\ell} \varepsilon(x_0 + r\cos\theta) \sin\theta \, d\theta. \tag{8}$$

The upper limit of the variable angle in the integral (8) is defined in such a way that θ_ℓ is either $\theta_\ell = 0$ for the case of a cloud entirely located outside the SCR (full line in figure 6(a)), i.e. $r \leqslant x_0 - w$, where w is the one side depleted layer width, or $\theta_\ell = \cos^{-1}[(x_0 - w)/r]$ when the cloud intercepts the SCR (dashed line in figure 6(a)), so that $r > x_0 - w$. This latter case leads, as mentioned above, to the dissociation and the subsequent loss of excitons and/or drops entering the concerned region.

Using $t = \cos\theta$ and the unified notation $b_m(r) = \mathrm{Min}[1, (x_0 - w)/r]$, we can rewrite (8) as follows:

$$E(r, x_0) = \int_{-b_m(r)}^1 \varepsilon(x_0 + rt) \, dt. \tag{9}$$

Taking into account the variation of ε according to (4), we obtain:

$$E(r, x_0) = \varepsilon_0[1 + b_m(r)] + \alpha \exp(-x_0/\sigma)(\sigma/r)\{\exp[r b_m(r)\sigma] - \exp(-r/\sigma)\}. \tag{10}$$

Introducing (10) in (7), the detailed integration of the intensity has been performed for the case of drops whose density is expressed by (6). This has given the following expression:

$$I(x_0) = I_0 + B\exp(-x_0/\sigma) - (I_0/2)\exp[-(x_0 - w)^3/L_{eff}^3] + (3I_0/2)\left(\frac{x_0 - w}{L_{eff}}\right)\Im$$
$$+ C\Im[\exp(-w/\sigma) - \exp(-x_0/\sigma)] \tag{11}$$

where

$$I_0 = \frac{2\pi}{3} n_0 L_{eff}^3 \varepsilon_0 \tag{12}$$

$$C = \pi\alpha\sigma L_{eff}^2 n_0 \tag{13}$$

$$B = 2C \int_0^\infty \exp(-u^3) \sinh(L_{eff} u/\sigma) u \, du \tag{14}$$

$$\Im = \int_{(x_0 - w)/L_{eff}}^\infty \exp(-u^3) u \, du \tag{15}$$

and using $u = r/L_{eff}$ as a variable representing the reduced length.

For a spot position, x_0, situated beyond the denuded zone, the recorded intensity $I(x_0)$ is merely I_0, the first term of the right-hand side of (11). When the denuded zone is reached and as long as the excitation beam is far from the boundary, so that $(x_0 - w) \gg L_{eff}$ is satisfied, the expression of $I(x_0)$ is reduced practically to the first two terms of (11), and this gives a clear account of the luminescence yield variation in this area. It is worth noting that I_0 is an experimental datum while B and σ can both be deduced from the fit of the part of the experimental curve corresponding to the enhancement of the PL emission arising from the denuded zone.

However, upon penetrating the SCR by the laser spot (figure 7), a new situation is created which accounts for the non-emissive character of the SCR (due to the instantaneous dissociation of the potentially photogenerated drops in this region by the built-in electric field). This aspect requires an appropriate correction of the intensity as calculated so far according to (11). In order to determine the related corrective factor, we assume a gaussian distribution of the intensity within the incident beam such as:

$$L(r_s) = L_0 \exp[-2r_s^2/w_0^2] \tag{16}$$

where w_0 is the half-width at $1/e^2$ of the maximum and $r_s^2 = (x - x_0)^2 + y^2$, the lateral variable radius inside the spot. The integrated intensity is then:

$$I_C(x_0) = \int L(x, y) f(x)\, dx\, dy \tag{17}$$

where

$$f(x) = \begin{cases} 1 & \text{for } -\infty < x < -w \text{ and } w < x < \infty \\ 0 & \text{for } -w \leqslant x \leqslant w. \end{cases} \tag{18}$$

The detailed calculation leads to:

$$I_C(x_0) = I_\infty \left\{ 1 + (1/2)\mathrm{erf}\left[\frac{\sqrt{2}}{w_0}(x_0 - w)\right] - (1/2)\mathrm{erf}\left[\frac{\sqrt{2}}{w_0}(x_0 + w)\right] \right\} \tag{19}$$

where $I_\infty = (L_0 w_0^2 \pi)/2$ is just $I(x_0)$ of (11) which makes allowance for the luminescence efficiency at the beam position x_0 and the spatial distribution of drops in the cloud. The bracketed term is the required correction factor.

5. Discussion

We have focused our computation on the case of condensed excitons by using the specific distribution density of the droplets as given by (6). This has allowed the detailed calculation leading to expression (11) or (19) for the total intensity. The application of this approach to FEs is not straightforward since a spatial distribution expression of FEs, such as that of (6) for EHD, is not available. Despite this, one could suggest that, whatever the distribution density of the free radiative particles, the comparison of the displayed scan profiles of both EHDs and FEs in figure 3 enables one to infer that the expansion of FEs exceeds that of EHDs. Such a conclusion agrees with those suggested by earlier results and conferring to FEs a wide expansion [11] as well as a high mobility [40].

In performing the fitting procedure, we begin our simulation by the experimental tail of the luminescence enhancement in order to determine the two characteristic parameters B and σ appearing in the general relationship (11). This reproduction concerns mainly the average curve of the luminescence in this area, setting aside the observed smooth modulation whose origin is extremely difficult to be well established. Nevertheless, a previous study on the EHD luminescence spatial distribution in Ge [41] had shown that the intensity at the generation point for thin samples exhibited a slight local minimum instead of an expected maximum and that this minimum was more and more severe as the thickness diminished. These features were attributed to the interaction with the back surface of the crystal [41]. While the nature of this interaction was not specified in that work, it is tempting to correlate it with the factor put forward by Hensel and Dynes [42] and relating to the effect of 'backwind' of phonons diffusively scattered from the sample end. The modulation of our intensity recalls this structure and since it becomes, similarly, more noticeable as one approaches the interface (see for instance the experimental profile for 9 mW in figure 8), we tentatively suggest the assignment of such behaviour to some interaction with the boundary containing precipitates and acting as a surface. This interaction would be completely hidden once the cloud edge reaches the boundary area where the dissociation of condensed excitons and the subsequent decrease of the intensity starts to prevail, as mentioned above.

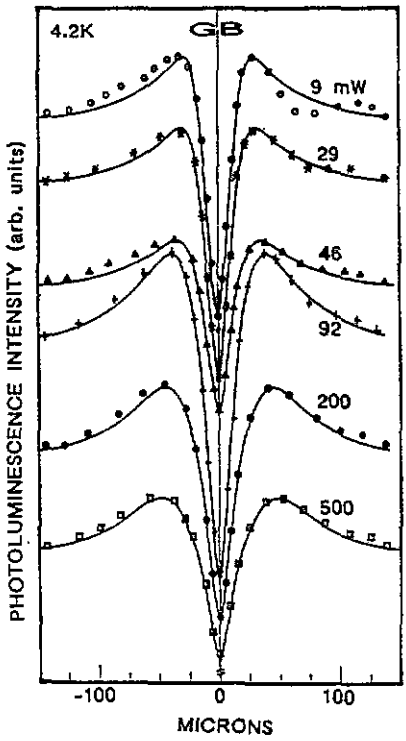

Figure 8. Scan profiles of the maximum intensity of the EHD emission across the grain boundary (GB) for the indicated pumping powers. The solid line is the calculated profile. For clarity the curves are shifted vertically.

The beginning of this decrease is very sensitive to the effective lateral extent of the cloud, L_{eff}, and, to a lesser extent, to the SCR width w. This last size is expected to retain,

theoretically, the same value for all the experimental runs, although some variation in w is quite conceivable from sample to sample or from one scan to another on various positions on the sample. That is the reason why the fitting values of w range within a narrow interval between 3 and 4 μm, which constitute anyhow a rough estimate of the actual value of w. This approach reduces strongly the number of fitting parameters and permits an accurate determination of L_{eff}, considering that the value of w_0, the spot width, does not affect the start of the decrease process and hence the value of L_{eff}, as long as it remains lower than it. In contrast, w_0 and w constitute both the determining factors for the adjustment of the minimum at the GB plane position.

The best fits are obtained for w of about 3-4 μm and a w_0 value ranging between 5 and 10 μm. Examples of comparison between the calculated and experimental scan profiles are displayed in figure 8 for the samples intentionally contaminated with copper and submitted to a laser power P ranging between 9 and 500 mW. This last value has been adopted as an upper limit for P in order to prevent any local heating of the sample. The various values of the remaining fit parameter L_{eff} used for the simulation of the profiles of figure 8 are displayed in figure 9, as a function of P. Also reported on the same plot (figure 9) are the fitting values of L_{eff} used for the reproduction of similar profiles (not shown here) recorded for the non-intentionally contaminated samples. The L_{eff} values were found to lie between ~ 20 and ~ 50 μm when P varies from 7 to 500 mW.

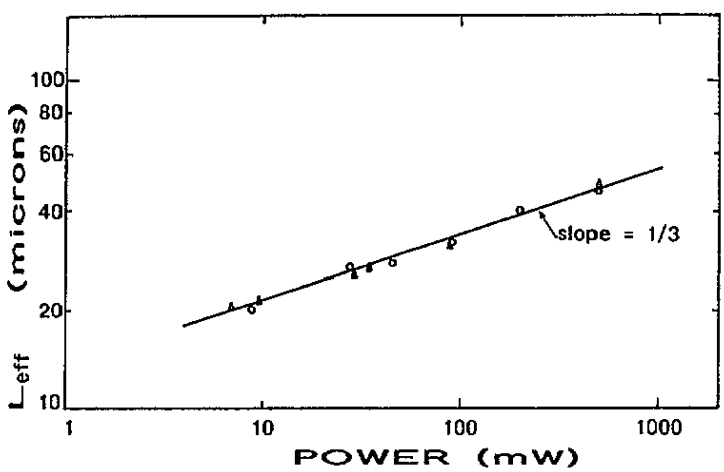

Figure 9. A log–log plot of the effective cloud expansion L_{eff} as a function of the laser power for the voluntarily contaminated samples (○) and the non-intentionally contaminated ones (△). The 1/3 slope value of the linear plot indicates a similar linear variation of the cloud volume with power.

We find that these parameters enable one to obtain a good description of the experimental profiles and provide, at the same time, a fairly good confirmation of the validity of the above-developed model.

According to the simple relation, $Q = 2qN_d w$, expressing the balance between the boundary charge density, Q (q is the elementary charge), and that of the depleted zone, a w fit value near 3–4 μm gives a Q value of a few 10^{11}e$^-$ cm^{-2}, quite consistent with the above-quoted average density of states of the boundary, as deduced from our transient capacitance measurements [21], where the so-called interface levels are assumed to be saturated by the

trapped carriers. On the other hand, the range of values inside which w_0 was found to lie (5–10 μm) could be ascribed to the approximations assumed for the modelling of the SCR effects, and also explained by the experimental errors associated with the handling of the focusing process which is hardly reproducible from one experiment to another.

Concerning the variation of the L_{eff} values with the laser power, as displayed in figure 9, one can easily note from the slope value (= 1/3) of the linear log–log plot a $P^{1/3}$ dependence of L_{eff}. Accordingly, the total volume of the EHD cloud increases linearly with the excitation level P. This implies a nearly constant average density of condensed excitons within the cloud. These findings are in good agreement with those reported previously for Si [13] and Ge [41, 43] where the filling factor f was found not to change with P and was estimated to be about 1%. This is a further confirmation of the configuration according to which the droplets are diffusively spread in the cloud, whereas earlier results on stressed Si [7] reported an increase of f with the excitation level to a value asymptotically approaching 1, i.e. a certain trend towards a large single drop. Compared to Ge [44, 45], the cloud expansion in Si is clearly much smaller and seems, to a certain extent, less anisotropic. Both characteristics have been correlated to the relative amounts of T and R phonons [18]. While the former (T) emanate from the point source at the sample surface where the laser is focused, the latter (R), due mainly to the Auger process in each droplet, are produced almost uniformly throughout the cloud. Owing to the greater contribution of R phonons in Si than in Ge resulting primarily from the larger average density [5], and since they reach a steady state after a much faster time (140 ns) in Si than in Ge (40 μs), the extension and shape of the cloud are expected to be much smaller and notably less anisotropic, respectively.

Unlike a previous study using a spot size as large as 35 μm [13] which constituted the imposed value to the cloud size at low excitation levels, the linearity of our plot in figure 9 up to the smallest value of P (7 mW) suggests that the entire extent of our spot is still well below the lowest value for L_{eff}($\sim$ 20 μm). Moreover, one may well wonder if the use of a larger multiline laser spot (110 μm) in the above-mentioned work [13] does not involve an unavoidable or artificial stretching of the cloud expansion. Consequently, we feel well founded in our thinking that our better spatial resolution has allowed, despite some uncertainties, a rather more accurate determination of the cloud lateral radius.

With the assumption that L_{eff} is the distance travelled by the EHD during its lifetime τ_0, as advanced earlier by Bagaev *et al* [17], one can estimate an average drift velocity of the droplet $v_d = L_{eff}/\tau_0$. For the range of values determined for L_{eff} and $\tau_0 = 140$ ns in Si, v_d evolves from 1.4×10^4 cm s^{-1} at low excitation to 3.5×10^4 cm s^{-1} at high excitation. This provides strong support to an EHD motion due to a phonon wind.

Turning to the scan profiles realized on the untreated A sample (figure 5), it is interesting to note that, of the above-described effects exerted by the GB in the annealed bicrystal, such as exciton dissociation and eventual subsequent carrier trapping which has led to a severe decrease of the PL intensity, none is apparently present in this case. This can be explained by the absence of barrier effects in the as-grown $\Sigma = 25$, quite compatible with the experimental observations [39] and theoretical calculations [46] which inferred a fully reconstructed boundary and the absence of associated localized states, respectively. A specific origin must then be explored for the striking feature of the counterbalancing behaviour of EHD and FE luminescence intensities, which starts at a few tens of micrometres from the interface but appears more pronounced when both phases are present (figure 5(*a*)) since it is greatly attenuated elsewhere (figure 5(*b*)). At first sight, it seems that a kind of phase exchange takes place between the condensed and gaseous states in the sense of a continuous rise of drop formation at the expense of the free particles up to the GB plane,

where both types of emission recover their bulk values. This could result from a certain shift of the gas–liquid coexistence line in a way more favourable to the formation of the liquid phase. This proposal of phase exchange occurrence is supported by the noticeable attenuation revealed (figure 5(*b*)) by each profile (particularly visible for EHD) upon removal of the opposite phase. The changes observed in figure 5(*a*) emerge at a distance representing approximately the average lateral radius of the cloud, i.e. when the cloud edge reaches the close vicinity of the GB where some lattice distortion prevails. Such distortion may originate from the array of primary dislocations characterizing the $\Sigma = 25$ GB [47]. On the other hand, previous investigations on Ge [48] and Si [7,27] have shown that a strain field gradient confines the droplets in points of maximum shear strain. This confinement is accompanied by a decrease of the average density of condensed excitons and a concomitant decrease of the EHD radiation intensity relative to the FE band [7,49]. In this context, one could regard the above-mentioned lattice distortion in the GB near-region as some *negative* strain which *raises* the formation of EHDs. However such an increase cannot happen unless this is done at the expense of FEs sustaining them, since the total generation rate would remain unchanged. This could be supported by recent results [50] reporting some unusual and random rise of the EHD line detected upon scanning an *as-grown* edge-defined film-fed growth (EFG) polycrystalline silicon. In the absence of possible correlation between this feature and any observable defect, the authors [50] suggested a possible origin lying in random stresses and strains inhomogeneously distributed in the EFG Si grains. In our opinion, it is highly likely that the random variation of the EHD line in the as-grown EFG material is due to the crossing of the multiple GBs by the excitation beam, which show similar influence on the EHD formation as that revealed by the GB of our as-grown bicrystal through the effects of lattice distortion in its vicinity. The modifications of the lattice environment near the GB would not be very large since no significant shift in the EHD and FE peak positions has been noticed [51]. The heat treatment leading to precipitate formation at the GB would result in the relaxation of the lattice in this area. Further experiments employing controlled strains on the boundaries of as-grown samples would be very useful to shed more light on the above-mentioned effects.

6. Conclusion

This paper presents an original application of the photoluminescence technique aimed at the investigation of the grain boundary effects in both annealed and as-grown $\Sigma = 25$ silicon bicrystals. The drastic decrease of the PL intensity of both EHD and FE emissions on both sides of the GB upon scanning the heat-treated specimens by the exciting laser beam has been explained by the dissociation of the radiative particles approaching the GB near-region. This dissociation has been ascribed to the built-in electric field that originates from the junction between the silicon grain and the metallic impurity precipitates at the GB plane. The smooth increase of the luminescence in the area adjacent to where the PL collapses has been correlated with the well-known gettering effect of the GB which leads to denuded zones free from non-radiative channels and contributes, therefore, to a consistent enhancement of the PL efficiency.

On the basis of the preceding scheme we have proceeded to a comprehensive modelling of the above-mentioned effects for the case of EHD droplets. Good simulations of the related profiles have been performed and the extracted best-fit parameters allow one to infer that:

(i) The slow increase of the effective lateral expansion of the cloud, L_{eff}, with the pumping power, P, follows a nearly $P^{1/3}$ variation. Such dependence indicates that we are dealing, firstly, with a somewhat isotropic cloud shape, and, secondly, with a cloud volume increasing nearly linearly with laser power. This latter aspect results then in an almost constant average pair density

(ii) The substantial rise of the average drift velocity of the droplets with P provides an additional support to the phonon wind model as a dominant origin of the droplet-transport mechanism.

Finally, for the as-grown sample, the opposite changes of EHD and FE intensities, as induced by the boundary, were tentatively interpreted in terms of the lattice distortion in the vicinity of the GB. More specific experiments are required for a more reliable explanation of this last aspect.

Acknowledgments

The technical assistance of P Voivenel and H Cubero is gratefully acknowledged. This work is partially supported by the EC contract No SC1*-CT91-0703 (TSTS).

References

[1] Governor C R M 1985 *J. Phys. C: Solid State Phys.* **18** 4079
[2] Strunk H P, Werner J H, Fortin B and Bonnaud O (ed) 1994 *Polycrystalline Semiconductors III—Physics and Technology (Solid State Phenomena, vols 37-38)* (Zürich: Trans Tech)
[3] Sauer R, Weber J, Soltz J, Weber E R, Küsters K-H and Alexander H 1985 *Appl. Phys.* A **36** 1
[4] Wijaranakula W 1991 *J. Appl. Phys.* **70** 3018
[5] Rice T M, Hensel J C, Phillips T G and Thomas G A, 1977 *Solid State Physics* vol 32, ed H Ehrenreich, F Seitz and D Turnbull (New York: Academic) pp 1–314
[6] Voos M, Leheny R F and Shah J 1980 *Handbook on Semiconductors: Optical Properties of Solids* vol 2, ed M Balkanski (Amsterdam: North-Holland) p 329
[7] Gourley P L and Wolfe J P 1981 *Phys. Rev.* B **24** 5970
[8] Wolfe J P 1982 *Phys. Today* **35** 46
[9] Mattos J C V, Shaklee K L, Voos M, Damen T C and Worlock J M 1976 *Phys. Rev.* B **13** 5603
[10] Bagaev V S, Zamkovets N Y, Keldysh L V, Sibel'din N N and Tsvetkov V A 1976 *Zh. Eksp. Teor. Fiz.* **70** 1501 (Engl. Transl. 1976 *Sov. Phys.–JETP* **43** 783)
[11] Martin R W 1974 *Phys. Status Solidi* b **61** 223 and references therein
[12] Capizzi R W, Voos M and Benoît à la Guillaume C 1975 *Solid State Commun.* **16** 709
[13] Tamor M A and Wolfe J P 1980 *Phys. Rev.* B **21** 739
[14] Voisin P, Etienne B and Voos M 1976 *Phys. Rev. Lett.* **42** 526
[15] Benoît à la Guillaume C, Voos M and Salvan F 1972 *Phys. Rev.* B **5** 3079
[16] Keldysh L V 1976 *Pis. Zh. Eksp. Teor. Fiz.* **23** 100 (Engl. Transl. 1976 *Sov. Phys.–JETP Lett.* **23** 86)
[17] Bagaev V S, Keldysh L V, Sibel'din N N and Tsvetkov V A 1976 *Zh. Eksp. Teor. Fiz.* **70** 702 (Engl. Transl. 1976 *Sov. Phys.–JETP* **43** 362)
[18] Markiewicz R S 1980 *Phys. Rev.* B **21** 4674
[19] The bicrystals have been grown by Cristaltec, Centre d'Etudes Nucléaires de Grenoble, France
[20] Broniatowski A 1989 *Phys. Rev. Lett.* **62** 3074
[21] Rizk R, Portier X, Nouet G and Allais G 1994 *J. Appl. Phys.* **76** 952
[22] Rizk R, Ihlal A and Portier X 1995 *J. Appl. Phys.* **77** 1875
[23] Rizk R, Cruège F, Madelon R and Nouet G 1994 *Proc. 3rd Int. Workshop on Beam Injection Assessment of Defects in Semiconductors (BIADS'93)* ed A Cavallini, C Donolato, and S Pizzini; 1994 *Mater. Sci. Eng.* B **24** 184
[24] Dash W C and Newman R 1955 *Phys. Rev.* **99** 1151
[25] Madelon R, Ajroudi M and Fortini A 1991 *Semicond. Sci. Technol.* **6** 810
[26] Shah J, Combescot M and Dayem A H 1977 *Phys. Rev. Lett.* **38** 1497

[27] Forchel A, Laurich B, Wagner J, Schmid W and Reinecke T L 1982 *Phys. Rev.* B **25** 2730
[28] Hammond R B, McGill T C and Mayer J W 1976 *Phys. Rev.* B **13** 3566
[29] Sparks D R and Chapman R G 1986 *J. Electrochem. Soc.* **133** 1201
[30] Aucouturier M, Broniatowski A, Chari A and Maurice J L 1989 *Polycrystalline Semiconductors (Springer Proceedings in Physics 35)* ed H J Möller, H P Strunk and J H Werner (Berlin: Springer) pp 64–76
[31] Huff H R, Abe T and Kolbesen B (ed) 1986 *Semiconductor Silicon* (Pennington, NJ: Electrochemical Society) pp 845–998
[32] Weber J, Bauch H and Sauer R 1982 *Phys. Rev.* B **25** 7688
[33] Vouk M A and Lightowlers E C 1975 *J. Phys. C: Solid State Phys.* **8** 3695
[34] Broniatowski A 1987 *Phys. Rev.* B **36** 5895
[35] Broniatowski A and Haut C 1990 *Phil. Mag. Lett.* **62** 407
[36] Elkajbaji M, Dessus J and Thibault J 1992 *Phil. Mag.* A **66** 873
[37] Evans J H, Kanienski J, Kanienski M and Rimmer J S 1992 *Semicond. Sci. Technol.* **7** A41
[38] Hvam J M and Balslev I 1975 *Phys. Rev.* B **11** 5053
[39] Bourret A and Rouvière J L 1989 *Polycrystalline Semiconductors (Springer Proceedings in Physics 35)* ed H J Möller, H P Strunk and J H Werner (Berlin: Springer) pp 8-18
[40] Tamor M A and Wolfe J P 1980 *Phys. Rev. Lett.* **44** 1703
[41] Kamerman G W and Feldman B J 1976 *Phys. Rev.* B **13** 5615
[42] Hensel J C and Dynes R C 1977 *Phys. Rev. Lett.* **39** 969
[43] Greenstein M and Wolfe J P 1978 *Phys. Rev. Lett.* **41** 715; 1980 *Solid State Commun.* **33** 309
[44] Markiewicz R S, Greenstein M and Wolfe J P 1980 *Solid State Commun.* **35** 339
[45] Greenstein M and Wolfe J P 1981 *Phys. Rev.* B **24** 3318
[46] Sutton A P 1989 *Inst. Phys. Conf. Ser.* **140** 13
[47] D'Anterroches C and Bourret A 1984 *Phil. Mag.* A **49** 783
[48] Markiewicz R S, Wolfe J P and Jeffries C D 1977 *Phys. Rev.* B **15** 1988
[49] Kulakovskii V D, Timofeev V D and Edel'stein V M 1978 *Zh. Eksp. Teor. Fiz.* **74** 372 (Engl. Transl. 1978 *Sov. Phys.–JETP* **47** 193)
[50] Sawyer W D and Michel J 1992 *Proc. 16th Int. Conf. on Defects in Semiconductors* ed G G DeLeo, M Stavola and G Davis; *Mater. Sci. Forum* **83-87** 291–6
[51] Yasutake K, Umeno M, Kawabe H, Nakayama H, Nishino T and Hamakawa Y 1982 *Japan. J. Appl. Phys.* **21** 1715